Supporting Information

Charge Transfer-Modulated Transparent Supercapacitor Using Multidentate Molecular Linker and Conductive Transparent Nanoparticle Assembly

Jimin Choi†, Donghyeon Nam†, Dongyeeb Shin†, Youngkwon Song†, Cheong Hoon Kwon†, Ikjun Cho†, Seung Woo Lee,‡ and Jinhan Cho*,†,*

† Department of Chemical and Biological Engineering, Korea University, 145 Anam-ro, Seongbuk-gu, Seoul 02841, Republic of Korea

‡ School of Mechanical Engineering, Georgia Institute of Technology, Atlanta, Georgia 30332-0245, United States

* seung.lee@me.gatech.edu

* jinhan71@korea.ac.kr

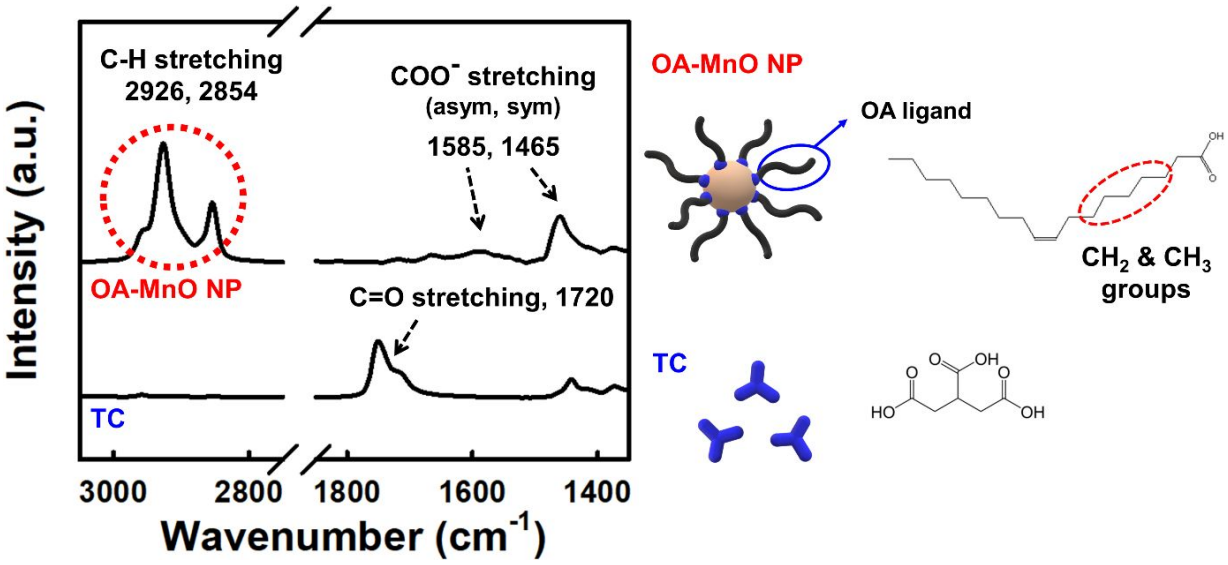

Figure S1. FTIR spectra of pristine OA-MnO NP and TC. In case of the OA-MnO NP, the COO^- stretching peak (at 1585 and 1465 cm^{-1}) appears in place of the C=O stretching (at 1710 cm^{-1}) peak from the COOH group and the C–H stretching peaks (ca. 2,926 and 2,854 cm^{-1}) derived from the long alkyl chain of OA ligands are shown. In case of the TC, any distinct peak does not appear in those ranges.

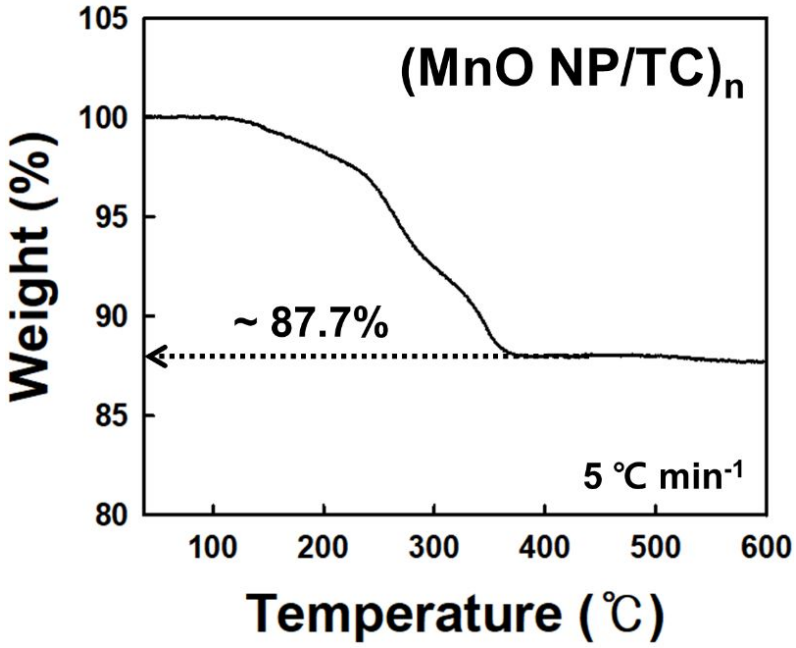

Figure S2. TGA profile of $(MnO\ NP/TC)_n$ multilayers with a heating rate of 5 ℃ min^{-1} under nitrogen environment. The composition of organic linkers is measured as approximately 12.3 %.

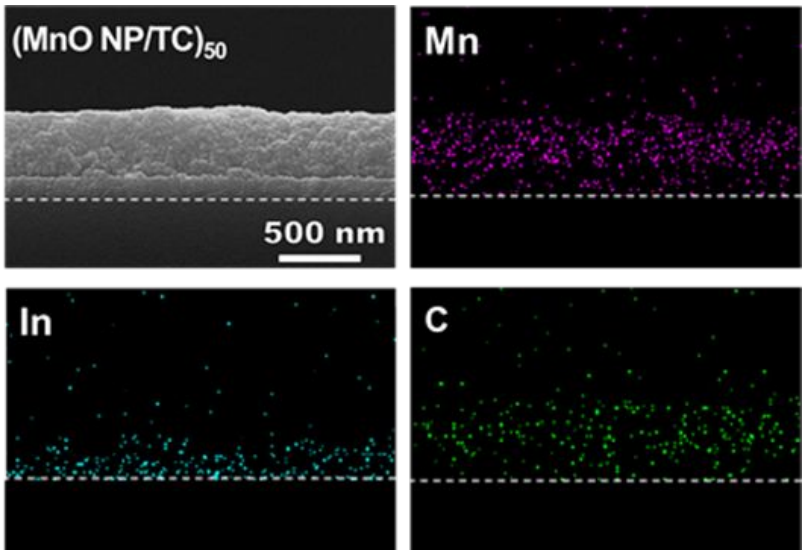

Figure S3. FE-SEM and EDS mapping images of the $(MnO\ NP/TC)_{50}$ multilayer with the thickness of 417 nm, assembled on the ITO glass

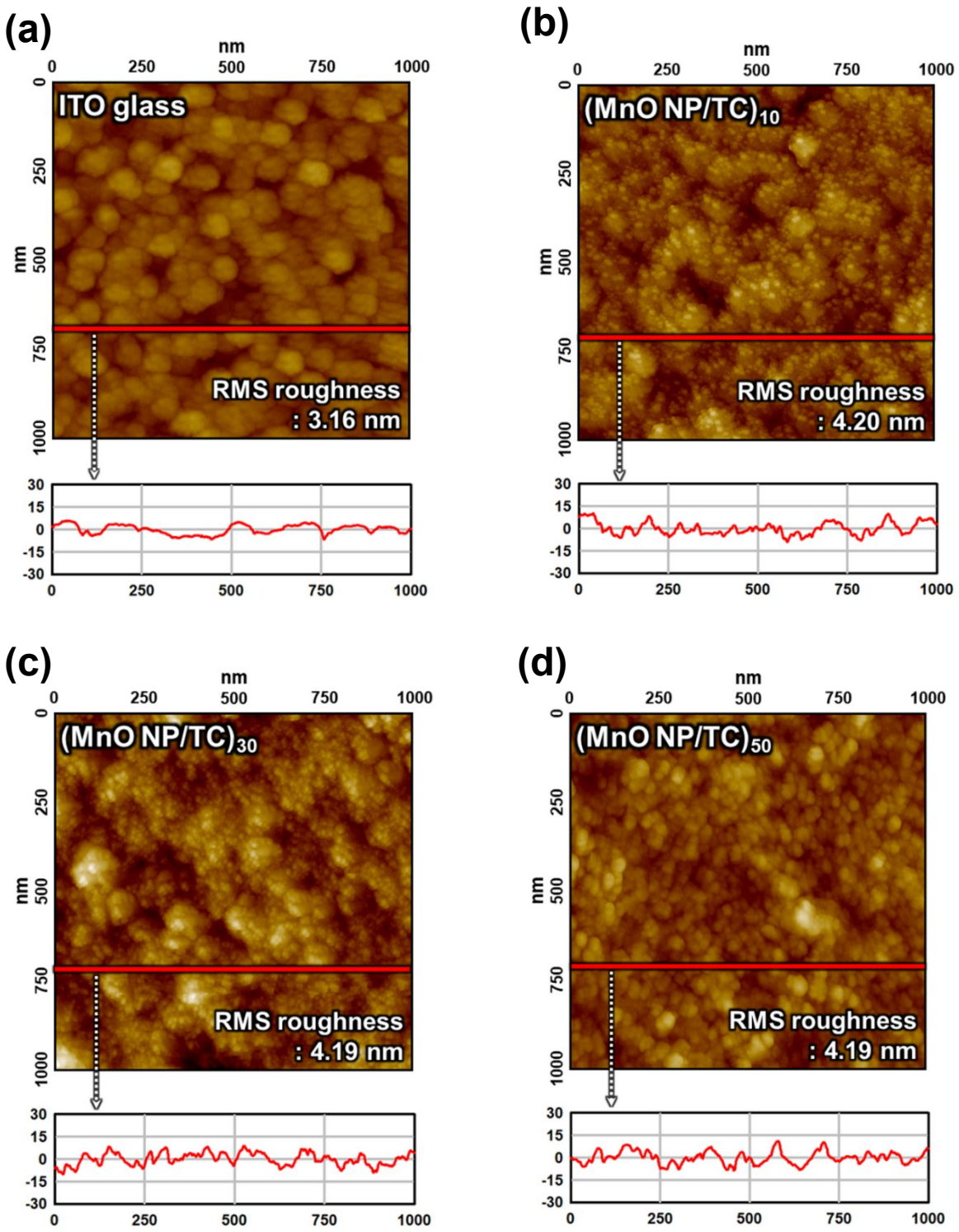

Figure S4. AFM images and surface roughness profiles of a) ITO glass, b) $(MnO\ NP/TC)_{10}$, c) $(MnO\ NP/TC)_{30}$ and d) $(MnO\ NP/TC)_{50}$ multilayers deposited onto the ITO glass.

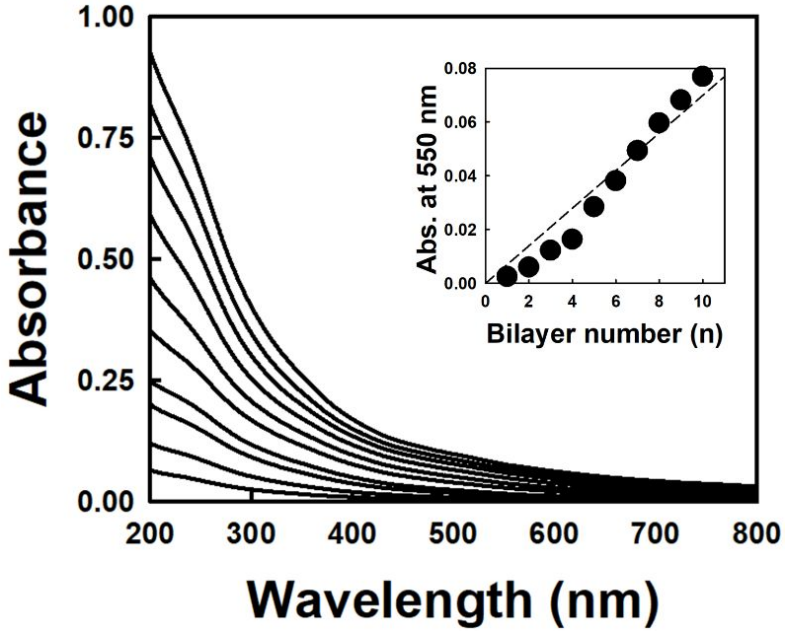

Figure S5. UV-vis absorbance spectra of (MnO NP/TC)$_n$ multilayers on quartz glasses as a function of bilayer number. The inset shows the absorbance at a wavelength of 550 nm, indicating the linear growth of multilayers.

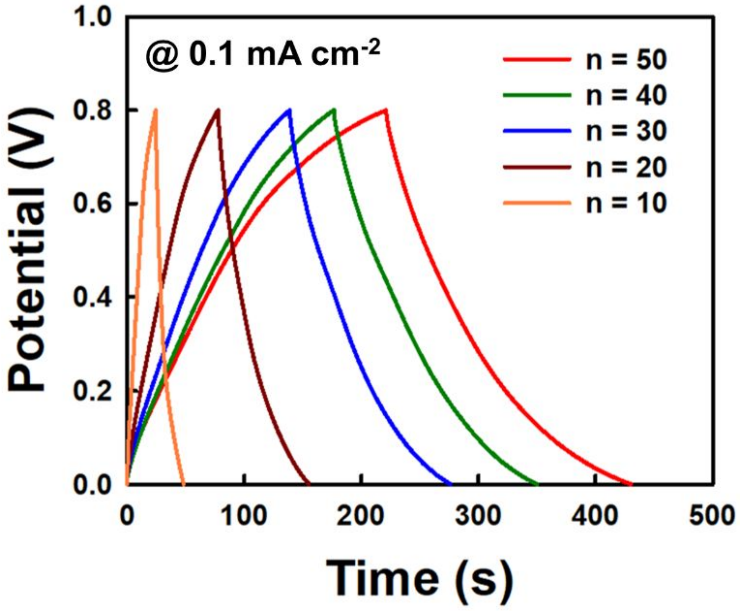

Figure S6. GCD profiles of the $(MnO\ NP/TC)_n$ electrodes as a function of the bilayer number (n) at a current density of 0.1 mA cm^{-2}.

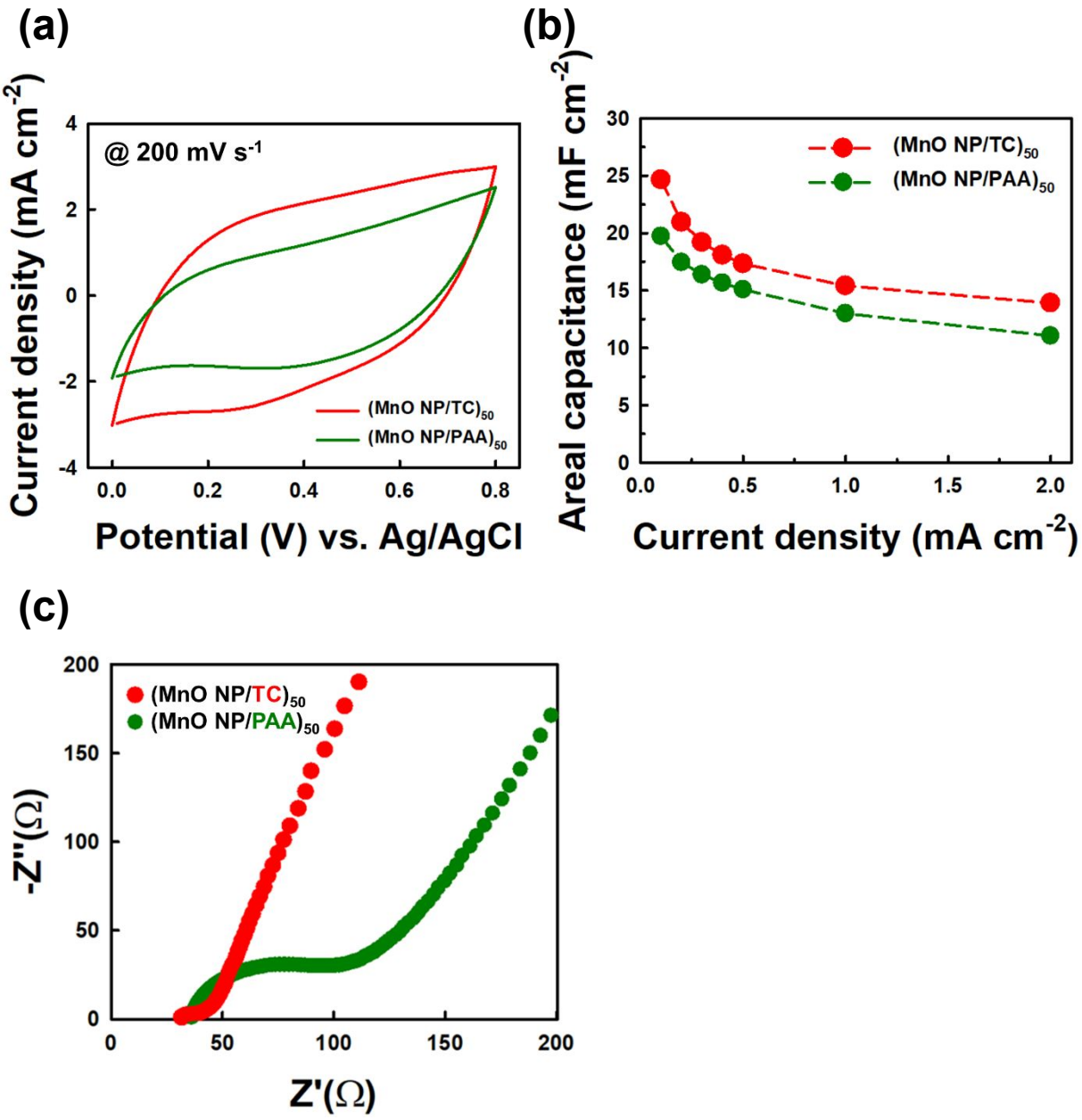

Figure S7. a) CVs of the $(MnO\ NP/TC)_{50}$ and $(MnO\ NP/PAA)_{50}$ electrodes at a scan rate of 200 mV s^{-1} and b) the areal capacitances of $(MnO\ NP/TC)_{50}$ and $(MnO\ NP/PAA)_{50}$ electrodes with increasing current density from 0.1 to 2 mA cm^{-2}. c) Nyquist plots of the $(MnO\ NP/TC)_{50}$ and $(MnO\ NP/PAA)_{50}$ electrodes.

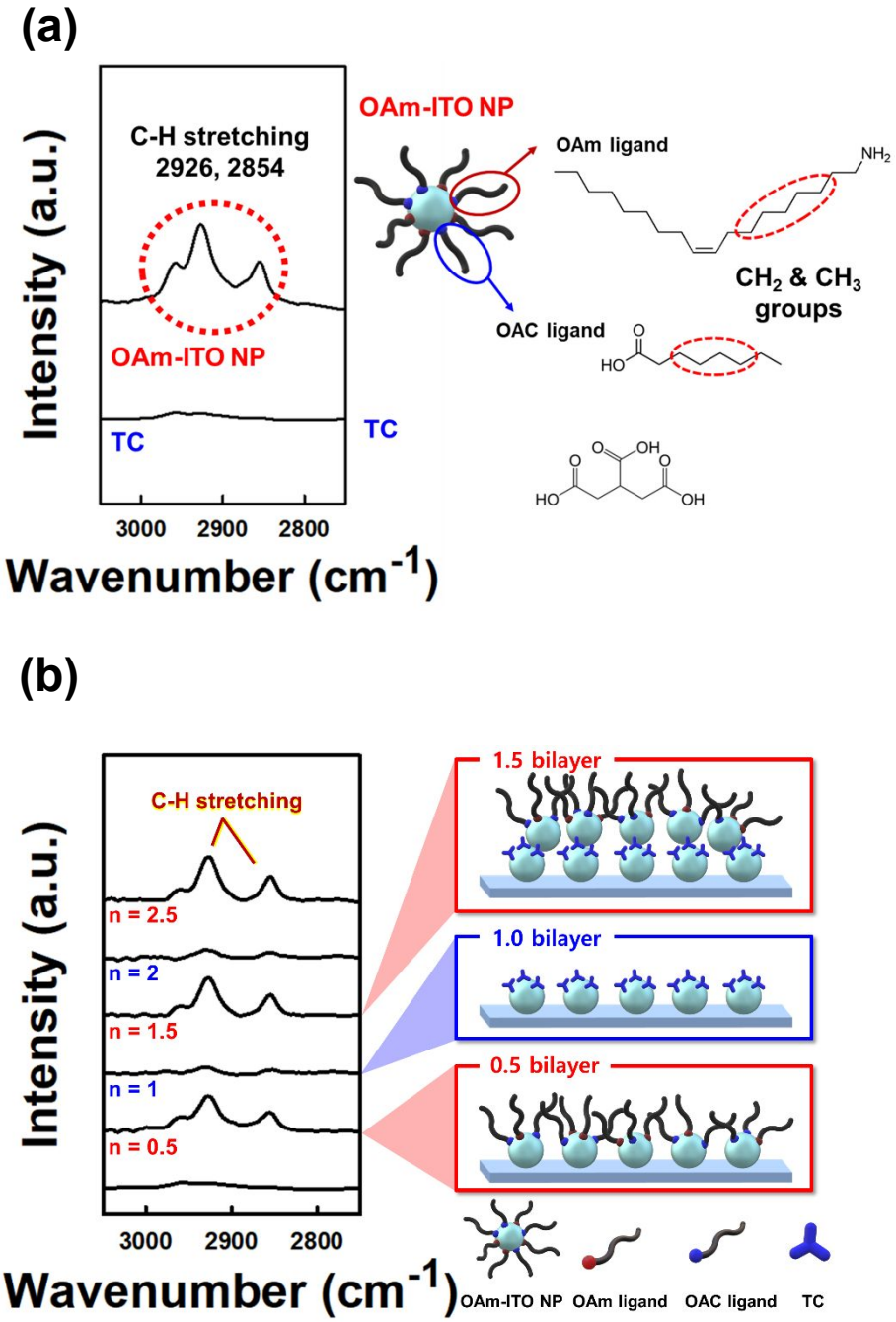

Figure S8. a) FTIR spectra of pristine OAm-ITO NP and TC. In this case, the C–H stretching peaks (at 2,926 and 2,854 cm^{-1}) originate from the long alkyl chain of OAm ligands and on the other hand, any distinct peak does not occur from TC. The scheme shown in the right side of b) displays LbL assembly process based on ligand exchange reaction between OAm-ITO NP and TC.

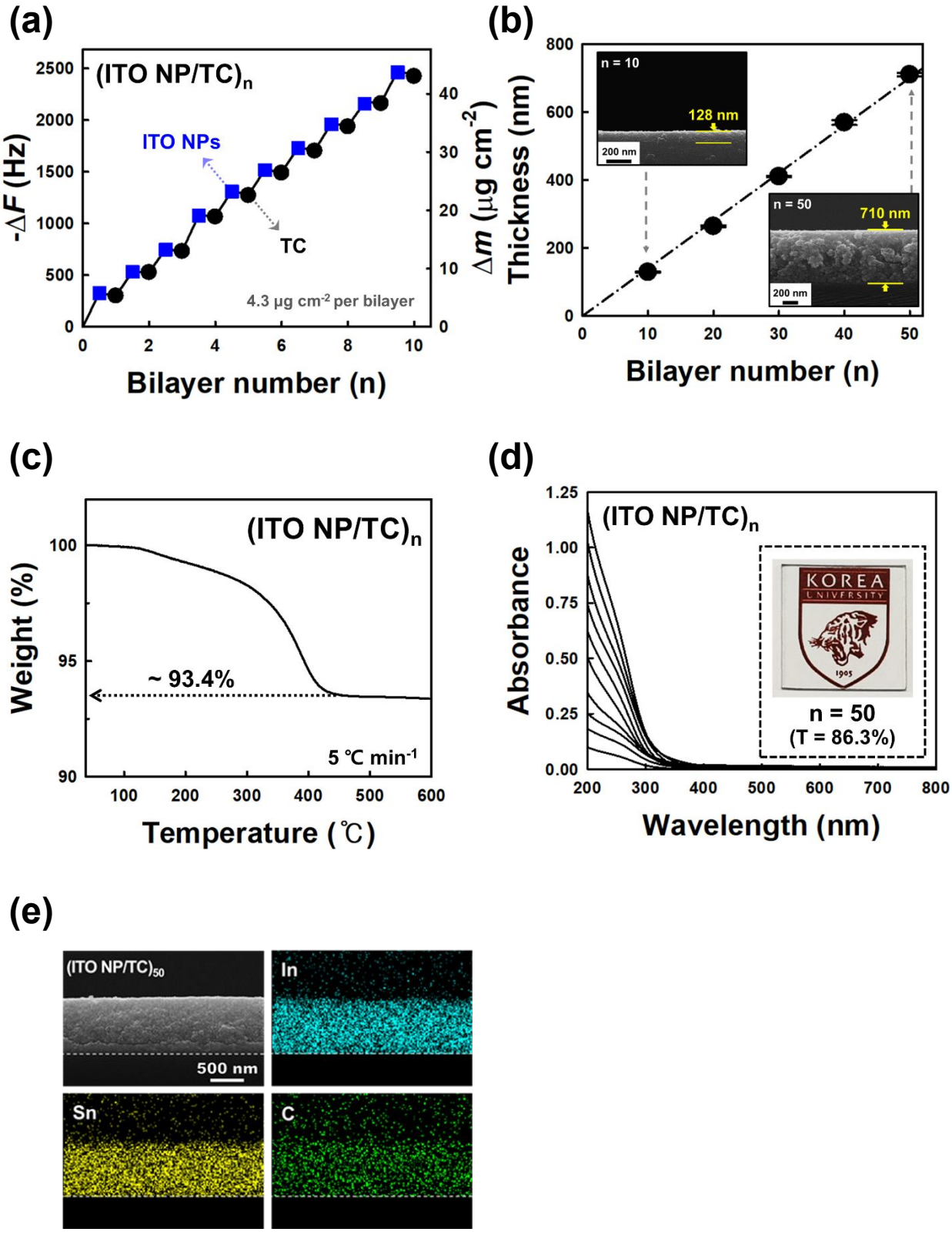
(a)
(ITO NP/TC)n
ITO NPs
TC
4.3 μg cm-2 per bilayer
-ΔF (Hz)
Δm (μg cm-2)
Bilayer number (n)
(b)
n = 10
128 nm
200 nm
n = 50
710 nm
200 nm
Thickness (nm)
Bilayer number (n)
(c)
(ITO NP/TC)n
~ 93.4%
5 ℃ min-1
Weight (%)
Temperature (℃)
(d)
(ITO NP/TC)n
KOREA UNIVERSITY
1905
n = 50
(T = 86.3%)
Absorbance
Wavelength (nm)
(e)
(ITO NP/TC)50
500 nm
In
Sn
C

Figure S9. a) Frequency and mass change of (ITO NP/TC)$_n$ multilayers obtained from the QCM measurements as a function of bilayer number. b) Thickness change of (ITO NP/TC)$_n$ multilayers onto Si-wafer measured from the cross-sectional FE-SEM images (insets). c) TGA profile of (ITO NP/TC)$_n$ multilayers. The composition of organic linkers is measured as approximately 6.6%. d) UV-vis absorbance spectra of the (ITO NP /TC)$_n$ multilayers on quartz glasses. The inset is the digital image of the (ITO NP/TC)$_{50}$ electrode with the transmittance of 86.3% at 550 nm. The university logos were used with permission from KOREA University. e) FE-SEM and EDS mapping images of the (ITO NP/TC)$_{50}$ with a thickness of 697 nm, assembled on the ITO glass

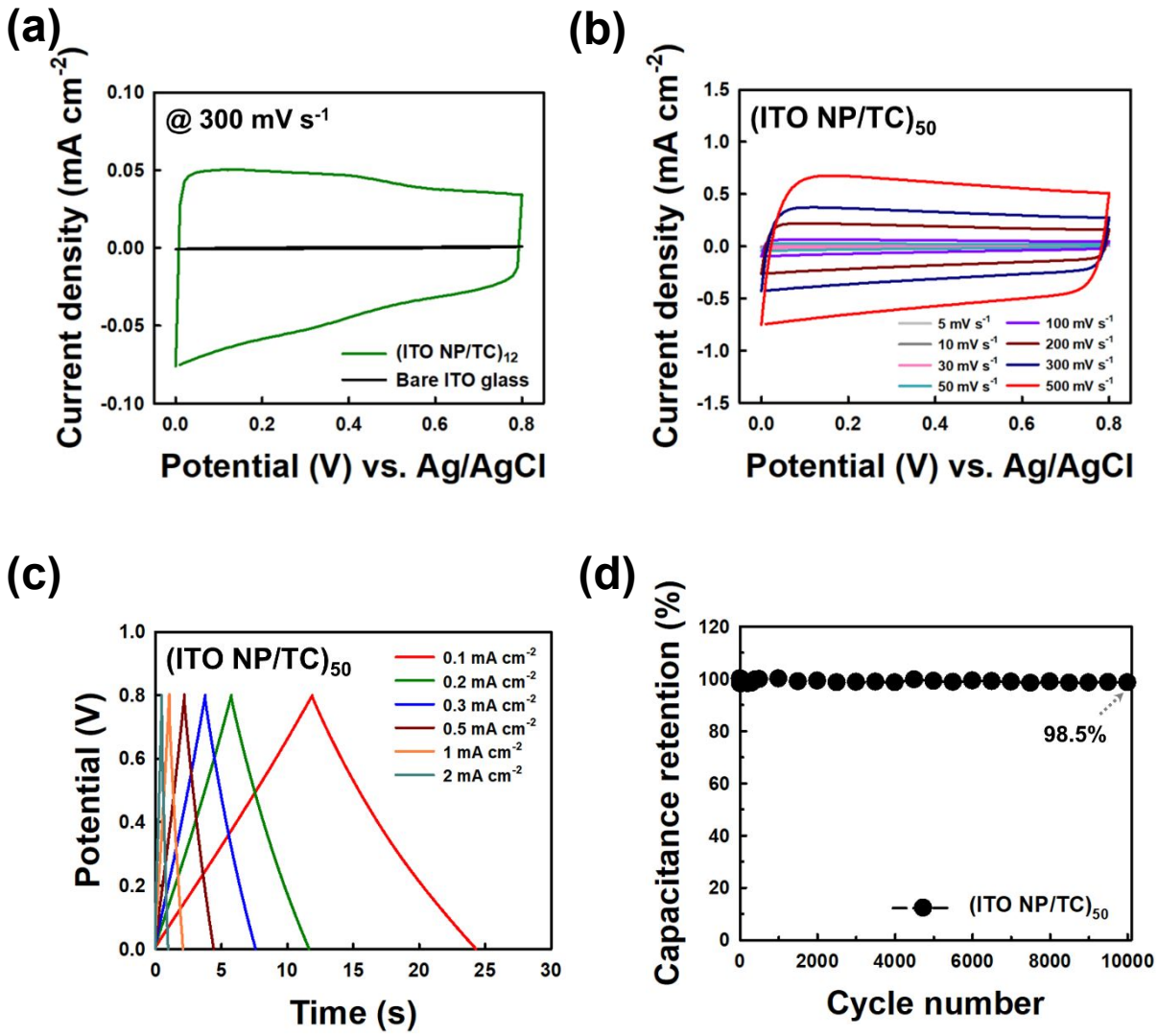

Figure S10. a) CVs of the bare ITO glass and the $(ITO\ NP/TC)_{12}$ on the ITO glass at a scan rate of 300 mV s^{-1}. b) CVs of the $(ITO\ NP/TC)_{50}$ electrode measured at 5-500 mV s^{-1}. c) GCD curves of the $(ITO\ NP/TC)_{50}$ electrodes at various current densities in the range of 0.1-2 mA cm^{-2}. d) Cycling retention of the $(ITO\ NP/TC)_{50}$ electrode during GCD at 2 mA cm^{-2}.

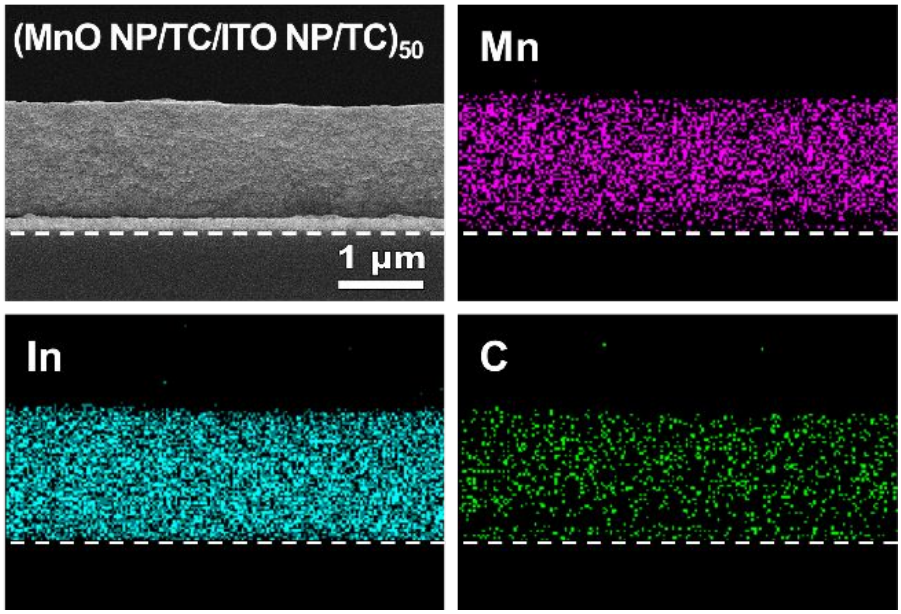

Figure S11. FE-SEM and EDS mapping images of the $(MnO\ NP/TC/ITO\ NP/TC)_{50}$ multilayer with the thickness of 1.3 μm, assembled on the ITO glass

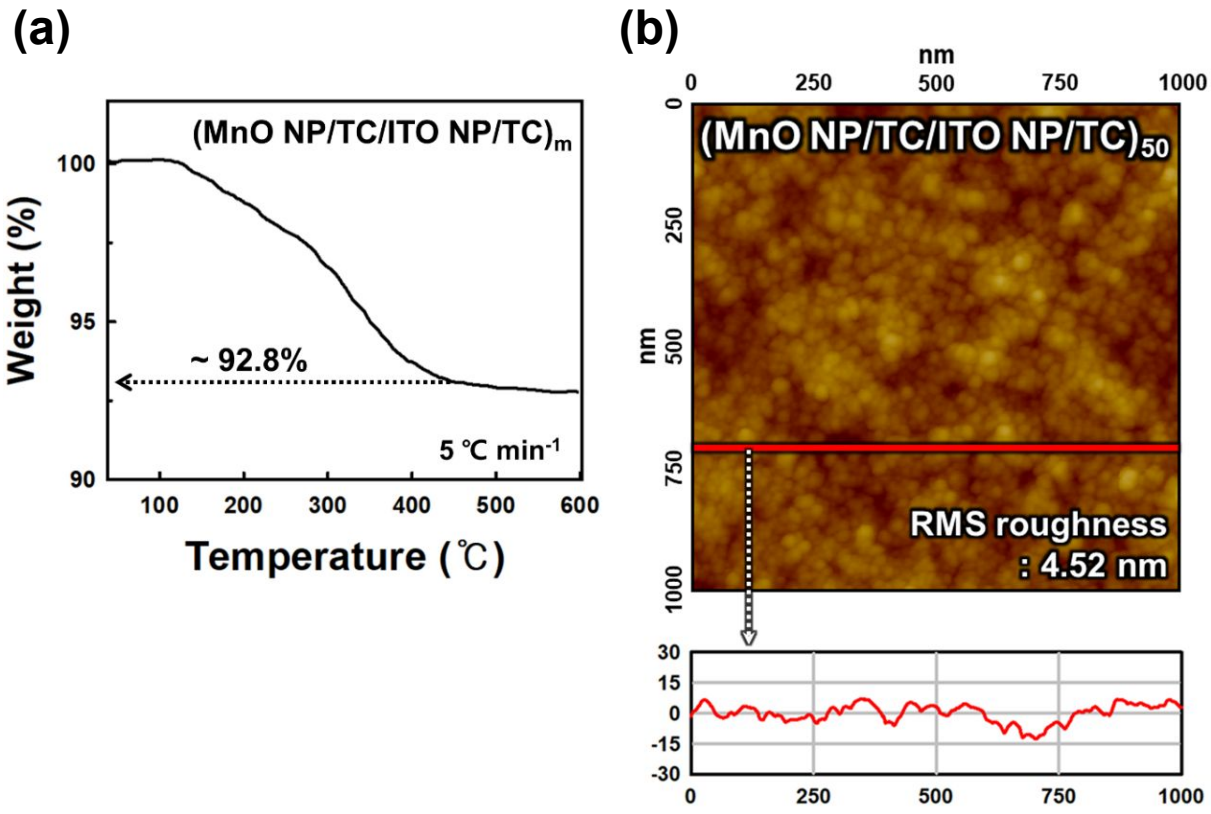

Figure S12. a) TGA profile of (MnO NP/TC/ITO NP/TC)$_m$ multilayers with a heating rate of 5 ℃ min $^{-1}$ under nitrogen environment. The mass ratio of organic linkers within multilayers is measured as approximately 7.2 %. b) AFM images and surface roughness profile of (MnO NP/TC/ITO NP/TC)$_{50}$ multilayer deposited onto the ITO glass.

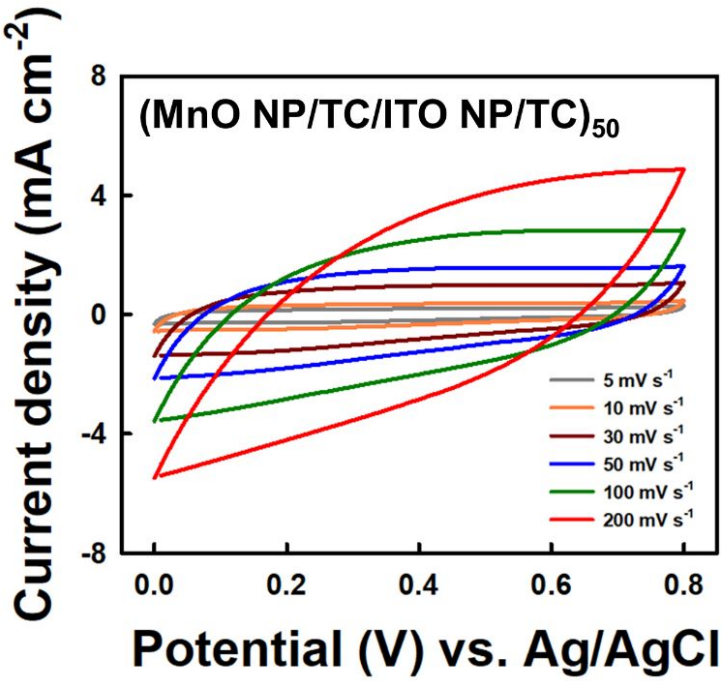

Figure S13. Scan-rate-dependent CVs of the (MnO NP/TC/ITO NP/TC)$_{50}$ electrode measured at 5-200 mV s^{-1}.

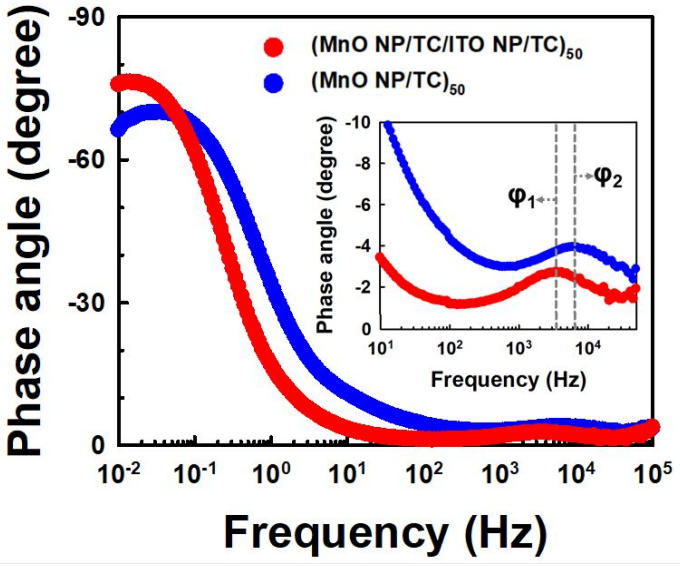

Figure S14. Bode plots of the (MnO NP/TC/ITO NP/TC)$_{50}$ and (MnO NP/TC)$_{50}$ electrodes in the frequency range from 100kHz to 0.01 Hz at a potential amplitude of 5 mV.

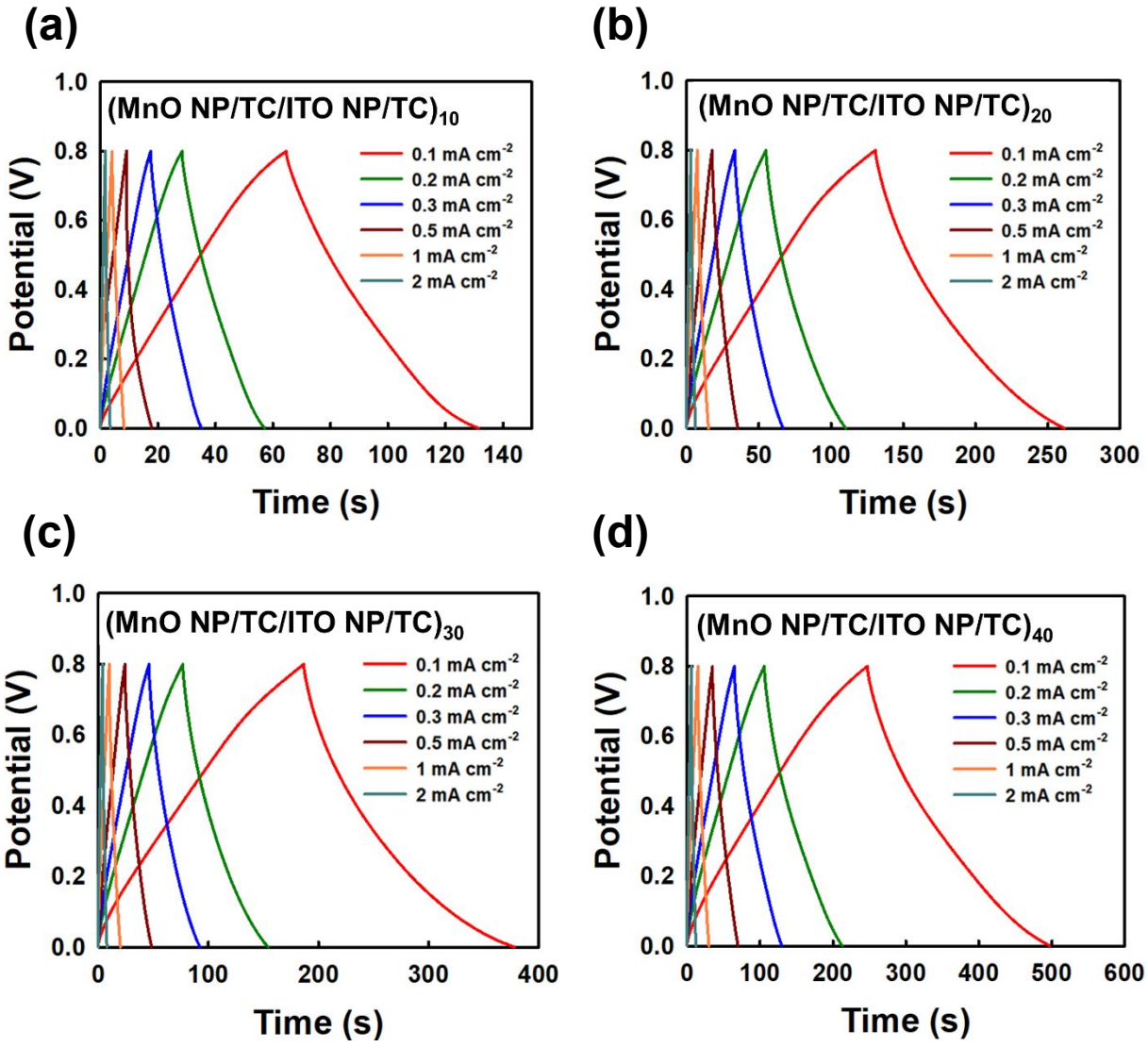

Figure S15. GCD profiles of (MnO NP/TC/ITO NP/TC)$_m$ multilayers at the applied current densities ranging from 0.1 to 2 mA cm^{-2} as a function of periodic number. a) m = 10, b) m = 20, c) m = 30, d) m = 40.

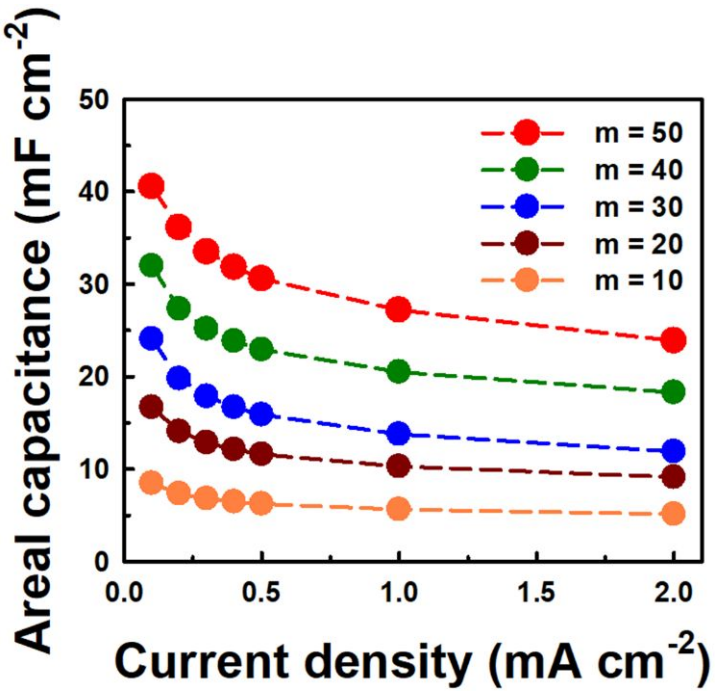

Figure S16. Areal capacitances of the (MnO NP/TC/ITO NP/TC)$_m$ electrodes at various current densities in the range of 0.1 to 2 mA cm^{-2}.

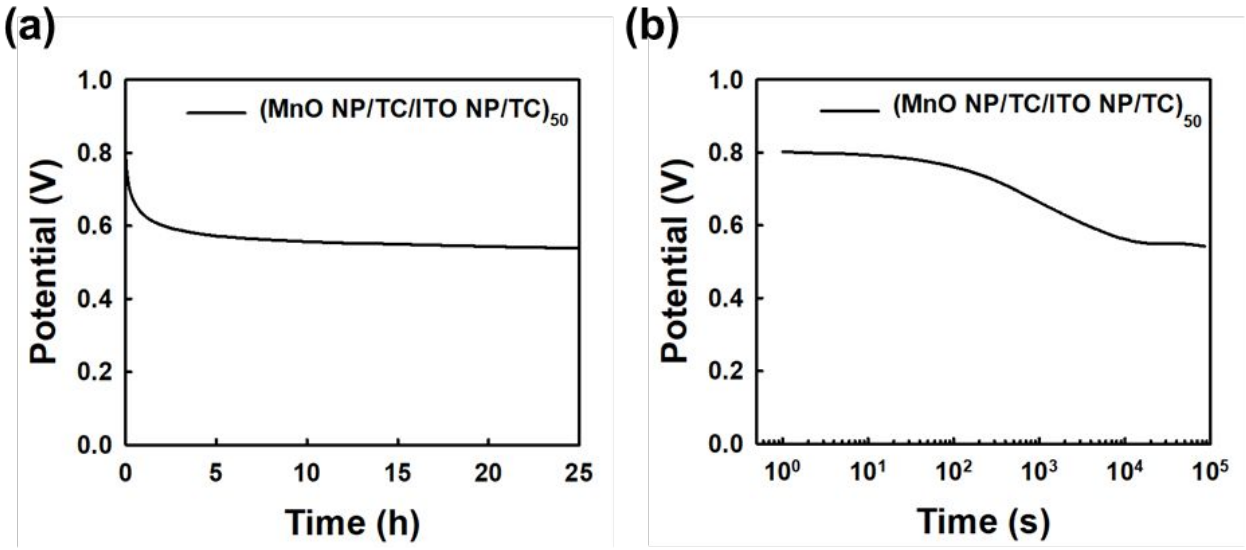

Figure S17. a) Self-discharge curve and b) logarithm of time-dependent self-discharge curve of the (MnO NP/TC/ITO NP/TC)$_{50}$ electrode obtained immediately after charging in 0.8 V in 0.5 M Na_2SO_4.

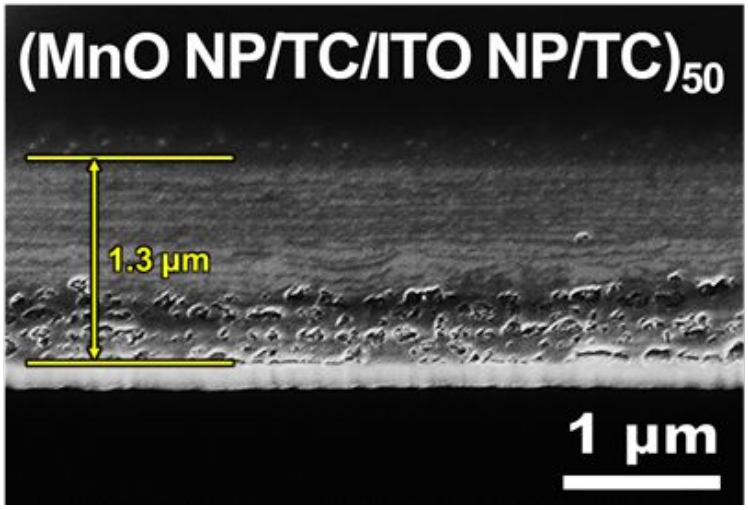

Figure S18. FIB-SEM image of the 1.3 μm thick-$(MnO\ NP/TC/ITO\ NP/TC)_{50}$ multilayers on the ITO coated PET substrate (sputtered ITO thickness: 160 nm)

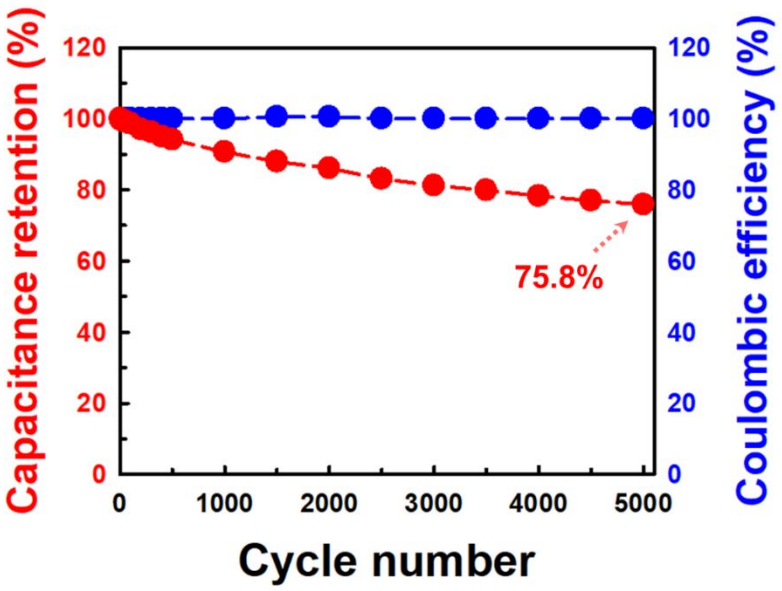

Figure S19. Cycling retention of the full-cell TSC device during GCD measurements at 0.5 mA cm^{-2}.

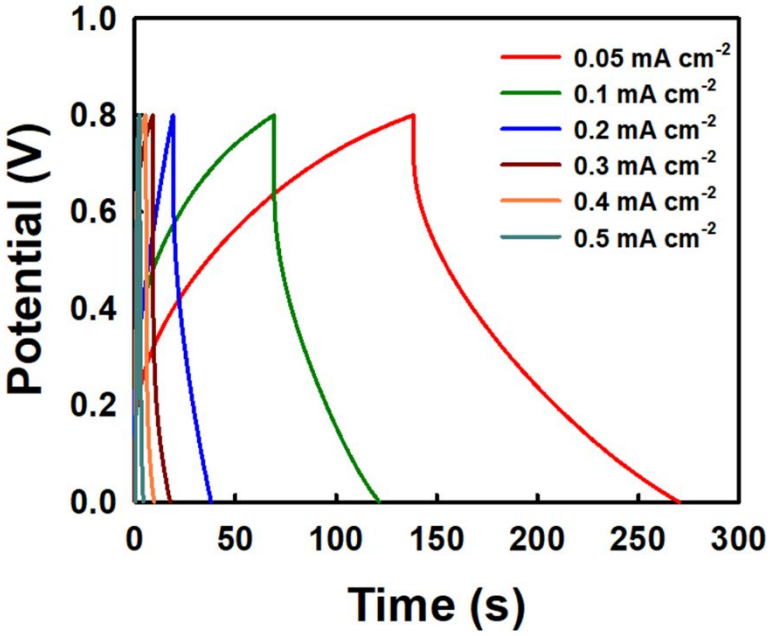

Figure S20. The GCD curves of the FS-TSC device under 180° bending condition.

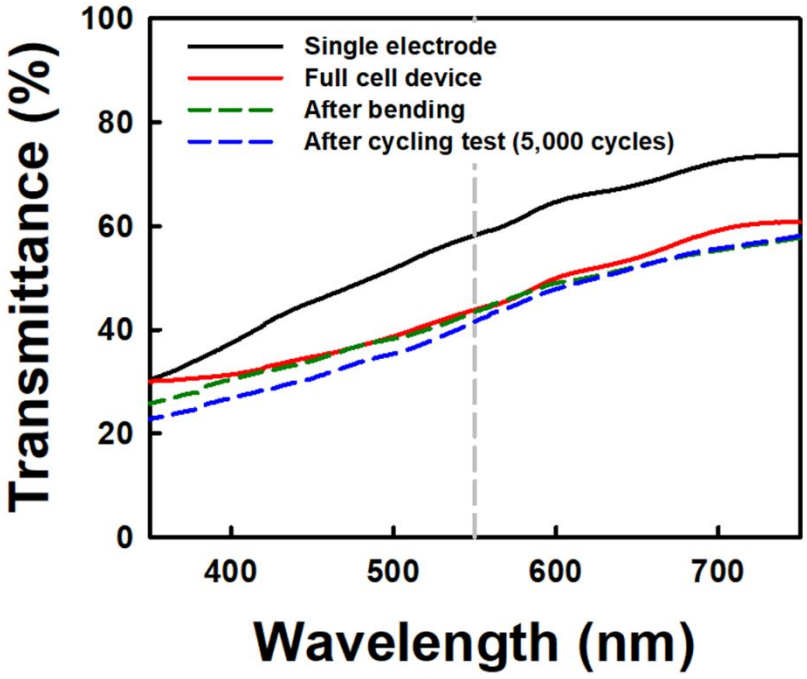

Figure S21. Transmittance spectra of the full-cell TSC device after bending and cycling test.

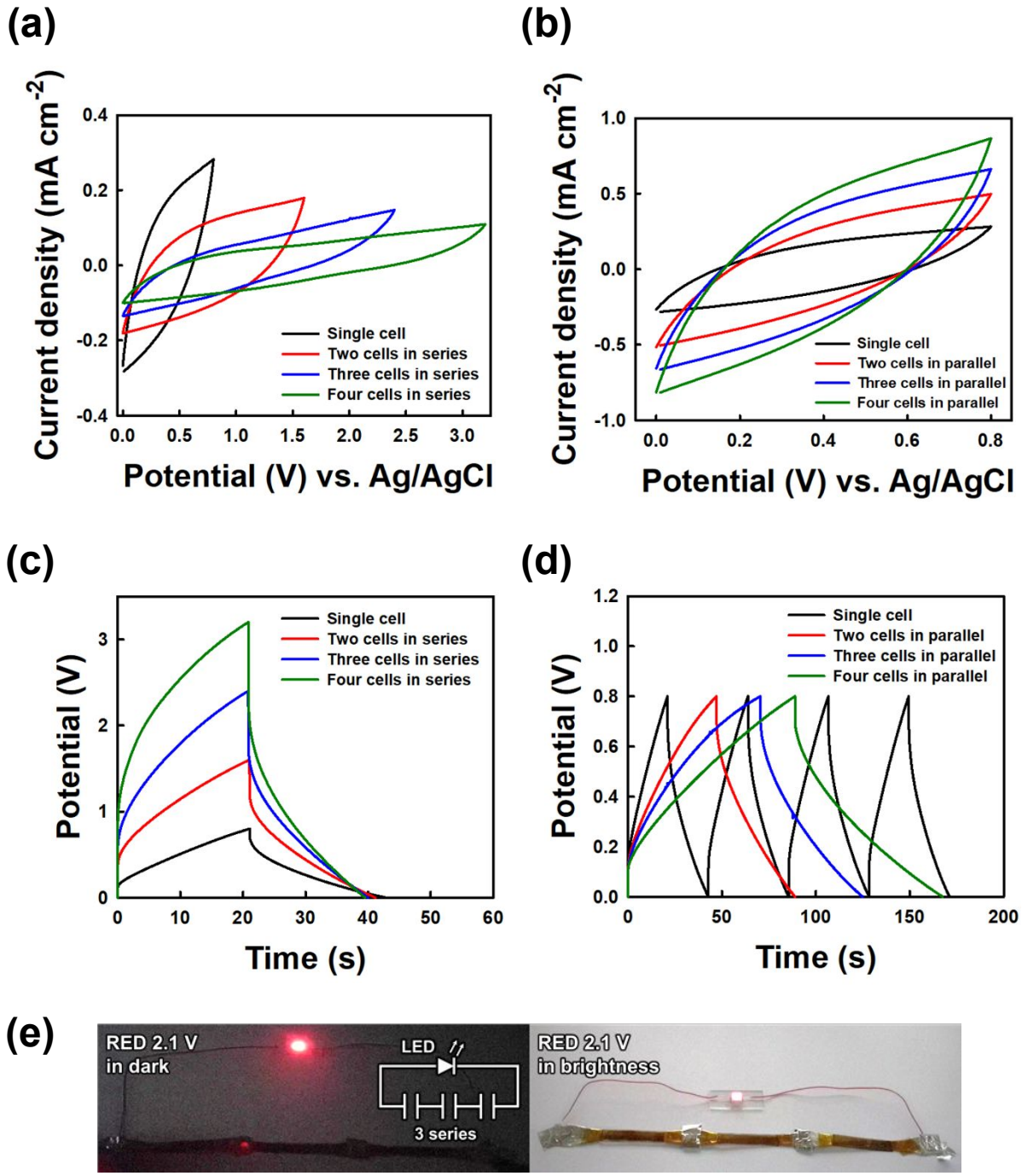

Figure S22. Full cell devices connected in series and parallel. a) and b) CV curves measured at a scan rate of 50 mV s^{-1} for four cells connected in series and parallel. c) and d) GCD curves measured at a current density of 0.2 mA cm^{-2} four cells connected in series and parallel. e) the digital images of LED operated by three full cells connected in series.